

Follow-Your-Preference++: Rethinking Preference Alignment for Image Inpainting

Junkun Yuan^{1*} Yutao Shen^{2*} Toru Aonishi² Hideki Nakayama² Yue Ma^{3†}
¹Zhejiang University ²The University of Tokyo ³Tsinghua University

*Equal contribution. †Corresponding author.

Abstract

We study preference alignment for image inpainting. Rather than proposing yet another method, we revisit the problem from first principles and reassess its core challenges. We adopt the widely used direct preference optimization framework and construct preference training data with publicly available reward models. Our empirical study spans nine reward models, two benchmarks, and two baseline inpainting models that differ in architecture and generative mechanism. Our main findings are: (1) Most reward models provide valid signals for preference data construction, although some are unreliable as evaluators. (2) Across models and benchmarks, preference data exhibits consistent trends under both candidate and sample scaling. (3) Reward models display pronounced biases—particularly in brightness, composition, and color scheme—that make them prone to inducing reward hacking. (4) A simple ensemble of reward models mitigates such biases and yields robust, generalizable performance. (5) Preference alignment is transferable to the object removal task, where the goal shifts from open-ended creative generation to coherent background completion. (6) Further analysis reveals that a calibrated ensemble method further mitigates hacking and improves robustness. Without modifying model architectures or introducing additional datasets, our models substantially outperform prior state-of-the-art models on standard metrics, large vision-language model evaluations, and human assessments. Our code is available at: <https://github.com/shenyttzzz/Follow-Your-Preference>.

1. Introduction

Image inpainting [5] aims to reconstruct user-specified regions of an image so that the completed result is visually coherent with the surrounding context and photorealistic. It underpins a wide range of applications, including photo restoration [30], content creation [80], and image editing [77]. Driven by the rapid progress in diffusion mod-

els [21] and flow-based models [32], image inpainting has become a prominent research direction.

Aligning visual generation systems with human preferences has recently emerged as a central research focus [6, 13, 61, 72]. Despite the substantial progress of image inpainting [23, 47, 69, 80], comparatively little effort has been devoted to aligning inpainting outputs with human preferences.

This paper studies preference alignment for image inpainting. Given the limited prior work on this task, our goal is not to introduce yet another method, but to revisit its fundamental questions. To this end, we adopt the widely used Direct Preference Optimization (DPO) [34, 51, 61] as the basis of our analysis for its simplicity and efficiency. To avoid the high cost and limited scalability of human annotation, we construct preference training data using publicly available, off-the-shelf reward models. Our investigation centers on three core questions: (1) How *effective* are these reward models at scoring candidates and constructing high-quality preference data? (2) How *scalable* is preference data with respect to candidate quantity and sample quantity? (3) How does *reward hacking* [48] arise, and how can it be mitigated?

To address these questions, we conduct experiments across *nine commonly used reward models* (e.g., HPSv2 [70], PickScore [25]), *two representative benchmarks* (BrushBench [23], EditBench [66]), and *two baseline inpainting models* (BrushNet [23], FLUX.1 Fill [8]) that cover diverse architectures (U-Net [53], Transformer [60]) and generative paradigms (diffusion [21], flow matching [32]). Our results show that: **(1)** Most reward models yield *valid* reward signals for constructing effective preference training data, although some of them are unreliable as evaluators and share common biases. **(2)** Across baselines and benchmarks, preference data exhibits *consistent trends* under both candidate scaling and sample scaling; nevertheless, biases in certain reward models (e.g., HPSv2) can induce reward hacking and weaken the effectiveness of scaling. **(3)** We uncover clear biases in reward models—particularly in *brightness, composition, and color scheme*—that make them susceptible to reward hacking. For instance, HPSv2 favors images with bright illumination, intricate compositions, and vivid colors, whereas PickScore ex-



Figure 1. **Results of our model.** The inpainting outputs generated by our model are visually coherent, semantically aligned with text prompts, and consistent with human aesthetic preferences.

hibits the opposite tendency. Consistent with this, PickScore pairs well with BrushNet, which generates vibrant outputs, while HPSv2 pairs well with FLUX.1 Fill, which produces plainer ones. We further trace these biases to systematic differences in the training data used by different reward models. (4) A simple ensemble of these reward models exhibits strong versatility across baselines and yields balanced, aesthetically pleasing inpainting results. (5) Preference alignment also transfers effectively to object removal with only minor pipeline adaptations. (6) Going beyond the conference version [56], we study several **Ensemble** variants and find that the original **Ensemble** still suffers from reward hacking; we therefore propose a calibrated ensemble that calibrates reward models, mitigates bias-induced hacking, and further improves robustness.

A preliminary version of this work appeared at ICLR 2026 [56], with the primary focus on creative image generation in the inpainting setting. The present paper extends this line of research in three directions. *First*, we generalize preference alignment to *object-removal inpainting*, a more challenging setting that requires the completed background to be both structurally coherent and visually plausible. *Second*, we provide a more comprehensive analysis of the Ensemble method, studying weighting strategies across reward models and the efficiency gains brought by filtering out invalid reward signals. *Third*, we revisit the mathematical formulation of the conference-version Ensemble, show that it can be interpreted as a calibration across reward models, and integrate it into the IPO loss [3] to further mitigate reward hacking. Together, these extensions establish a new state-of-the-art over the conference version.

Based on this exploration, we build simple yet effective preference-aligned inpainting models via reward ensembling.

Without modifying model architectures or introducing new datasets, our models substantially outperform prior state-of-the-art models on standard metrics, large vision-language model evaluations, and human assessments. Qualitative comparisons further show that our models generate more coherent and visually appealing results than competing methods. We hope this work establishes a simple yet strong baseline that helps advance this promising research direction.

2. Related Work

Image inpainting [5] aims to restore missing or corrupted regions of an image by generating visually plausible and semantically coherent content that is well aligned with the surrounding context. The field has progressed rapidly [15, 47, 67, 75, 76], largely driven by the development of diffusion [21] and flow-based generative models [11, 12, 32, 39–43, 45, 46, 63]. These models progressively transform random noise into structured visual content through iterative denoising or rectified flow matching, thereby providing a powerful generative prior for synthesizing realistic and high-quality image regions. Building on these advances, pioneering efforts [2, 52, 78] have introduced such generative paradigms to image inpainting, and subsequent methods [23, 74, 80] have further improved architectural design, controllability, and generation quality under more challenging inpainting settings. For example, BrushNet [23] introduces a dual-branch architecture that explicitly decouples masked-image feature extraction from the subsequent generation process, enabling the model to better preserve contextual information while producing more flexible and effective inpainting results. FLUX [7], in contrast, is a rectified-flow transformer that exhibits strong image generation capability, producing visually appealing results with high fidelity. Its in-

painting variant, FLUX.1 Fill [8], serves as a strong baseline for high-quality content completion in masked regions.

Object removal can be viewed as a free-form image inpainting task, but with a stronger emphasis on seamless and plausible background completion rather than open-ended or creative generation. Its goal is to replace user-specified masked objects with realistic background content that is visually coherent with the surrounding context. Recent studies are predominantly built on diffusion and flow-based models [12, 21, 32, 58], and largely fall into two paradigms: inversion-based methods [19, 36] and training-based methods [10, 24, 29]. For instance, RORem [29] alternates between training a discriminator and optimizing a diffusion model with human annotators in the loop, ultimately yielding both a well-aligned diffusion model and a high-quality dataset for object removal.

Image generation with preference alignment is an emerging field that seeks to align synthesized images with human preferences [22, 73]. Earlier works [6, 13] employ reinforcement learning (RL) [59] to fine-tune generative models with feedback from reward models. More recent works explore methods built on Direct Preference Optimization (DPO) [51], which bypasses the explicit RL stage. For instance, Diffusion-DPO [61] is the first attempt to align diffusion-based generation with human preferences by optimizing a pairwise preference objective. CaPO [27] aligns diffusion models with multiple reward models by first calibrating the scores across reward models and matching the resulting calibrated reward differences via a regression loss. PrefPaint [35] refines image inpainting results using a reward model trained on human-annotated data.

3. Preliminaries

3.1. Diffusion Models and Flow-Based Models

Diffusion models [57, 58], such as DDPM [21], are a class of generative models that learn to reverse a gradual noise corruption process. DDPM assumes a forward process that gradually applies noise to real data. At timestep t , the real data x_0 is destroyed to x_t : $q(x_t|x_0) = \mathcal{N}(x_t; \sqrt{\bar{\alpha}_t}x_0, (1 - \bar{\alpha}_t)\mathbf{I})$, where $\bar{\alpha}_t$ is a noise scheduling hyper-parameter. It has a reparameterization formula: $x_t = \sqrt{\bar{\alpha}_t}x_0 + \sqrt{1 - \bar{\alpha}_t}\epsilon$, where noise $\epsilon \sim \mathcal{N}(0, \mathbf{I})$. DDPM learns a reverse process using a denoising model ϵ_θ with parameters θ , inverting the forward process: $p_\theta(x_{t-1}|x_t) = \mathcal{N}(\mu_\theta(x_t), \Sigma_\theta(x_t))$. The denoising model ϵ_θ can be trained by minimizing:

$$\mathcal{L}_{\text{DDPM}} = \mathbb{E}_{t,x_0,\epsilon} [\|\epsilon - \epsilon_\theta(\sqrt{\bar{\alpha}_t}x_0 + \sqrt{1 - \bar{\alpha}_t}\epsilon, t)\|^2]. \quad (1)$$

Flow-based models [12] are generative models that learn to model data distributions using invertible transformations. Recently, **Flow Matching** [32] has emerged as a prominent approach for visual generation [16, 37]. It usually learns a continuous-time flow that transforms a simple prior distribu-

tion into the data distribution by solving an ODE. The process, with an optimal-transport path, employs a linear interpolation scheme: $x_t = (1-t)x_0 + t\epsilon$. A denoising model v_θ is trained to predict the velocity field by minimizing:

$$\mathcal{L}_{\text{FM}} = \mathbb{E}_{t,x_0,\epsilon} [\|v_\theta((1-t)x_0 + t\epsilon, t) - (\epsilon - x_0)\|^2]. \quad (2)$$

U-Net [53] is used as the basic model structure by many previous denoising models [21, 58]. U-Net is a symmetric encoder-decoder architecture that captures multi-scale features through progressive downsampling and upsampling. **Transformers** [60], employed in recent works [16, 17, 26, 62], process all data elements in parallel using attention, facilitating training scalability.

To improve the reliability and generalization of conclusions drawn in our studies, we conduct investigations using two different **baseline models**—**BrushNet** [23] and **FLUX.1 Fill** [8], introduced in section 2. BrushNet is built on a U-Net-like architecture and trained with the DDPM loss, while FLUX leverages transformers and learns via Flow Matching.

3.2. Preference Alignment

The standard pipeline for training large-scale models typically involves pre-training, supervised fine-tuning, and preference alignment. Preference alignment refines model outputs to better match human values. Reinforcement Learning from Human Feedback (RLHF) [4] is a popular alignment approach. It utilizes human preferences on model outputs to train a *separate reward model*, which subsequently provides rewards for alignment via reinforcement learning algorithms such as PPO [55] and GRPO [18]. In comparison, **Direct Preference Optimization (DPO)** [51], which performs direct supervised learning, offers higher training efficiency. It constructs a preference dataset that comprises *preferred samples* and *dispreferred samples*. DPO learns human preferences implicitly contained within the data by maximizing:

$$\mathbb{E}_{x,y^w,y^l} [\log \sigma \left(\beta \log \frac{\pi_\theta(y^w|x)}{\pi_{\text{ref}}(y^w|x)} - \beta \log \frac{\pi_\theta(y^l|x)}{\pi_{\text{ref}}(y^l|x)} \right)], \quad (3)$$

where σ is the sigmoid function; π_θ and π_{ref} are the *policy* and the *reference policy*, respectively. In image generation, given a text prompt x , y^w and y^l denote the generated preferred image and dispreferred image, respectively. The hyper-parameter β controls the strength of regularization: a large value of β increases regularization pressure, dampening preference learning. In visual generation, Equation 3 can be derived to yield a simplified loss [34, 61]:

$$\mathcal{L}_{\text{DPO}} = -\mathbb{E} [\log \sigma (-\beta ((\mathcal{L}_\theta^w - \mathcal{L}_{\text{ref}}^w) - (\mathcal{L}_\theta^l - \mathcal{L}_{\text{ref}}^l)))], \quad (4)$$

where \mathcal{L}_θ^w and \mathcal{L}_θ^l denote the loss (Equation 1 or Equation 2) applied to the policy on preferred samples and dispreferred samples, respectively; similarly, $\mathcal{L}_{\text{ref}}^w$ and $\mathcal{L}_{\text{ref}}^l$ denote the losses applied to the reference policy. This loss

Table 1. Comparisons of reward models using **BrushNet** on BrushBench and EditBench.

reward model	CLIPScore		Aesthetic		ImageR		PickScore		HPSv2		VQAScore		UnifiedR		Perception		HPSv3		GPT-4	
	Brush.	Edit.	Brush.	Edit.	Brush.	Edit.	Brush.	Edit.	Brush.	Edit.	Brush.	Edit.	Brush.	Edit.	Brush.	Edit.	Brush.	Edit.	Brush.	Edit.
Baseline	26.415	27.337	6.425	5.392	12.717	-1.296	22.133	20.616	27.509	23.076	9.060	6.770	3.303	2.100	26.290	26.410	5.749	0.403	79.391	57.046
Random	26.441	27.631	6.424	5.392	12.685	-1.136	22.130	20.642	27.501	23.067	9.050	6.917	3.302	2.110	26.292	26.422	5.738	0.425	79.177	56.753
CLIPScore	26.461	27.710	6.430	5.393	12.782	-0.720	22.146	20.680	27.582	23.316	9.062	<u>6.894</u>	3.341	2.124	26.324	<u>26.548</u>	5.777	0.640	79.661	57.539
Aesthetic	26.465	<u>27.355</u>	<u>6.477</u>	5.520	<u>12.994</u>	-0.877	22.221	20.689	27.594	23.166	9.065	<u>6.828</u>	3.343	2.140	26.293	<u>26.342</u>	5.922	0.597	81.603	58.603
ImageR	26.471	<u>27.539</u>	6.462	5.434	12.891	-0.377	22.153	20.701	27.672	23.467	<u>9.036</u>	<u>6.761</u>	3.334	2.144	26.305	26.501	5.913	0.782	80.341	57.806
PickScore	<u>26.397</u>	<u>27.199</u>	6.454	5.454	12.893	<u>-1.364</u>	22.254	<u>20.732</u>	<u>27.322</u>	<u>22.933</u>	9.062	<u>6.873</u>	<u>3.353</u>	2.178	<u>26.273</u>	26.427	5.750	0.469	82.726	59.550
HPSv2	<u>26.481</u>	<u>27.677</u>	6.476	5.495	12.890	0.128	22.137	20.725	27.818	23.742	9.073	<u>6.818</u>	3.332	2.155	26.361	26.678	5.979	1.061	79.914	57.658
VQAScore	26.442	<u>27.524</u>	6.429	5.407	<u>12.658</u>	-0.800	<u>22.126</u>	20.667	27.527	23.234	<u>9.038</u>	<u>6.879</u>	3.311	2.139	26.326	<u>26.406</u>	<u>5.723</u>	0.555	<u>78.877</u>	<u>56.975</u>
UnifiedR	<u>26.428</u>	<u>27.505</u>	6.433	5.402	12.764	-0.812	22.157	20.675	27.562	23.204	9.061	<u>6.857</u>	3.329	2.155	26.320	26.436	5.800	0.540	80.333	57.185
Perception	26.448	<u>27.484</u>	6.428	5.393	12.789	-0.973	22.177	20.660	27.519	23.111	<u>9.069</u>	<u>6.894</u>	3.327	2.160	26.310	26.515	5.764	0.433	80.277	57.254
HPSv3	26.461	<u>27.547</u>	6.464	5.448	12.922	<u>-0.146</u>	22.176	20.713	27.758	23.491	9.065	<u>6.850</u>	3.344	2.158	26.317	26.535	<u>6.014</u>	0.863	80.623	57.485
Ensemble	26.535	<u>27.398</u>	6.485	<u>5.497</u>	13.037	-0.352	<u>22.229</u>	20.735	<u>27.797</u>	<u>23.522</u>	<u>9.053</u>	<u>6.892</u>	3.365	<u>2.176</u>	<u>26.338</u>	<u>26.603</u>	6.074	<u>1.015</u>	<u>82.172</u>	<u>58.986</u>

Bold values denote the best results. Underlined values denote the second-best results. Values in **blue** denote the results below the baseline or random chance.

Table 2. Comparisons of reward models using **FLUX.1 Fill** on BrushBench and EditBench.

reward model	CLIPScore		Aesthetic		ImageR		PickScore		HPSv2		VQAScore		UnifiedR		Perception		HPSv3		GPT-4	
	Brush.	Edit.	Brush.	Edit.	Brush.	Edit.	Brush.	Edit.	Brush.	Edit.	Brush.	Edit.	Brush.	Edit.	Brush.	Edit.	Brush.	Edit.	Brush.	Edit.
Baseline	26.244	27.103	6.429	5.458	12.760	4.910	22.327	21.211	27.476	24.076	9.081	8.012	3.360	2.485	25.945	26.834	6.055	2.470	83.935	66.979
Random	26.239	27.078	6.431	5.459	12.772	4.955	22.328	21.211	27.475	24.100	9.077	8.030	3.356	2.491	25.944	26.838	6.056	2.490	83.517	66.942
CLIPScore	<u>26.233</u>	<u>27.072</u>	6.432	5.477	12.791	4.997	22.329	21.215	27.487	24.121	<u>9.071</u>	8.071	3.361	2.512	25.948	26.859	6.056	2.499	83.942	66.997
Aesthetic	<u>26.250</u>	<u>27.200</u>	6.432	<u>5.478</u>	12.823	<u>5.175</u>	22.337	21.219	27.520	24.142	<u>9.075</u>	<u>8.001</u>	3.363	2.507	25.954	26.878	6.075	<u>2.577</u>	83.950	67.906
ImageR	26.251	27.121	6.434	5.481	12.823	5.001	22.336	21.211	27.518	24.143	<u>9.080</u>	<u>7.977</u>	3.362	<u>2.536</u>	25.946	26.846	6.078	2.550	84.176	67.785
PickScore	<u>26.236</u>	27.195	6.436	5.476	12.879	5.134	22.341	21.223	27.530	24.154	<u>9.076</u>	<u>8.003</u>	3.383	2.514	25.955	<u>26.900</u>	6.105	2.548	84.188	67.100
HPSv2	26.246	27.160	<u>6.441</u>	5.475	12.904	5.145	22.356	21.232	27.605	24.202	9.085	<u>8.028</u>	3.363	2.553	25.963	26.895	6.181	2.605	84.699	68.186
VQAScore	<u>26.243</u>	<u>27.101</u>	6.432	5.466	12.781	<u>4.926</u>	22.329	21.215	27.486	24.104	<u>9.075</u>	<u>8.020</u>	<u>3.353</u>	2.501	25.950	26.861	<u>6.046</u>	<u>2.473</u>	<u>83.854</u>	<u>66.793</u>
UnifiedR	<u>26.235</u>	27.133	6.434	5.473	<u>12.769</u>	5.034	22.331	21.212	27.485	24.120	<u>9.076</u>	<u>8.014</u>	3.366	2.517	25.954	26.853	6.057	2.524	83.950	67.372
Perception	26.251	<u>27.088</u>	6.433	5.466	<u>12.752</u>	4.975	22.331	<u>21.209</u>	27.479	24.109	9.082	<u>8.023</u>	<u>3.356</u>	2.514	25.951	<u>26.818</u>	6.064	2.504	84.022	68.024
HPSv3	<u>26.238</u>	27.223	<u>6.441</u>	5.465	12.855	5.092	22.340	<u>21.226</u>	27.534	<u>24.155</u>	<u>9.083</u>	<u>8.000</u>	<u>3.378</u>	2.497	<u>25.957</u>	26.859	6.106	2.568	84.615	<u>68.107</u>
Ensemble	<u>26.239</u>	27.158	6.442	5.472	<u>12.884</u>	5.239	<u>22.346</u>	21.215	<u>27.560</u>	24.146	9.082	<u>8.036</u>	3.367	2.507	25.963	26.905	<u>6.151</u>	<u>2.577</u>	<u>84.628</u>	67.549

Bold values denote the best results. Underlined values denote the second-best results. Values in **blue** denote the results below the baseline or random chance.

function aligns the distribution of generated samples with the preferred data distribution and encourages it to diverge from the dispreferred distribution. Due to the simplicity, efficiency, and stability of DPO, *this paper will explore preference alignment for image inpainting by optimizing Equation 4 on different preference datasets that are constructed for investigation.*

3.3. Reward Models

Reward models play an important role in preference alignment: they provide real-time rewards in RLHF [55], and offer scores for constructing offline preference data in DPO [27, 68]. However, prior works [64, 72] directly employ off-the-shelf reward models for visual preference alignment without systematic evaluation. In this paper, we evaluate the effectiveness of these reward models in constructing preference

data via extensive studies. Specifically, we examine the following **public reward models**: (1) **CLIPScore** [20] measures semantic alignment between images and text prompts by calculating cosine similarities of their CLIP embeddings [50]. (2) **Aesthetic** [54] predicts human aesthetic preferences on top of the CLIP embeddings. (3) **ImageReward (ImageR)** [71] is trained by fine-tuning BLIP [28] on 137K preference samples. (4) **PickScore** [25] is a CLIP-based image scoring model, trained on over 500K synthesized image samples with users’ preference choices. (5) **HPSv2** [70] is also a CLIP-based model that evaluates both image quality and text-image alignment by learning from 798K human preferences on 433K sample pairs. (6) **VQAScore** [31] provides a semantic alignment score by computing the probability of a VQA model answering “yes” to each question: “Does this figure show {text}?”. (7) **UnifiedReward (UnifiedR)** [68] is a unified model that assesses both visual generation and understanding. (8) **Perception Encoder (Perception)** [9] is trained by contrastive visual-language pre-training, producing semantically aligned multimodal embeddings. (9) **HPSv3** [44] is trained on 1.5M annotated sample pairs using Qwen2VL-7B [65].

To assess their efficacy, these models are employed to assign reward scores to candidate samples that are generated by the baseline models with different random seeds. The resulting highest- and lowest-scoring samples for each text prompt are subsequently utilized as the preferred and dispreferred samples for DPO training. Based on the evaluation of training results, the top-performing ones are designated as the most effective reward models to provide accurate rewards, whereas the lowest-performing models are designated as the least effective.

4. How Effective are Reward Models?

The ability of reward models to accurately predict human preferences is critical to the performance of preference alignment algorithms. To evaluate this capability, we apply DPO to the preference data constructed by the reward models and evaluate the model’s performance after training. Specifically, based on the popular dataset of BrushData [23], we generate 16 **candidate** inpainting results with varied random seeds for each prompt and the corresponding masked image. The candidates are scored by the reward models, and the highest-scoring (preferred) and lowest-scoring (dispreferred) samples form preference pairs for DPO training. Following [38, 68], the reward models are employed to serve two purposes: (1) *providing scores to construct training data*, and (2) *evaluating performance after training*. All experiments adhere to the same training configurations by default (e.g., a learning rate of $1e-7$, β of 2000, and 2000 training steps, etc.), with the only variation being the reward model used to score and construct the training data. Note that we may encounter an **oracle reward model** [38], where the same model

Algorithm 1: Ensemble Reward via Mean Rank

Input : \mathcal{I} : set of candidate images generated with different random seeds under the same prompt;
 \mathcal{M} : set of reward models;
 $s[m][i]$: reward score of image $i \in \mathcal{I}$ assigned by reward model $m \in \mathcal{M}$.
Output: Winning sample i^w and losing sample i^l .

```

1 begin
   // Step 1: rank candidates under
   // each reward model (rank 1
   // denotes the highest score).
2   for  $m \in \mathcal{M}$  do
3     Sort  $\{s[m][i]\}_{i \in \mathcal{I}}$  in descending order and let
   // rank[m][i] be the position of image i in the
   // sorted list;
4   end for
   // Step 2: average per-model
   // ranks to obtain the Ensemble
   // rank.
5   for  $i \in \mathcal{I}$  do
6     Ensemble[i]  $\leftarrow \frac{1}{|\mathcal{M}|} \sum_{m \in \mathcal{M}} \text{rank}[m][i]$ ;
7   end for
   // Step 3: select the best and
   // worst candidates (a smaller
   // Ensemble value indicates a
   // better candidate).
8    $i^w \leftarrow \arg \min_{i \in \mathcal{I}} \text{Ensemble}[i]$ ;
9    $i^l \leftarrow \arg \max_{i \in \mathcal{I}} \text{Ensemble}[i]$ ;
10 end

```

is used both for data construction and performance evaluation within one experiment. We assess results on two benchmarks, i.e., BrushBench [23] and EditBench [66].

Here, we introduce a new reward model—**Ensemble**—that selects preference pairs based on the mean rank across all reward models: for images generated with different random seeds under the same prompt, we rank the images under each reward model and average the per-model ranks of each image to obtain its Ensemble rank; we then select the highest-ranked image as the winning sample and the lowest-ranked image as the losing sample. The full procedure is summarized in Algorithm 1.

We make **GPT-4** [1] serve as a “fair” evaluator by assessing aesthetic quality, structural coherence, and semantic alignment of the results. Given GPT-4’s [1] strong multimodal understanding capabilities, we use it to evaluate image inpainting results. Specifically, we provide GPT-4 with (1) a system prompt, (2) an input image, (3) the mask to inpaint, (4) an inpainting prompt, (5) and the inpainting result. The

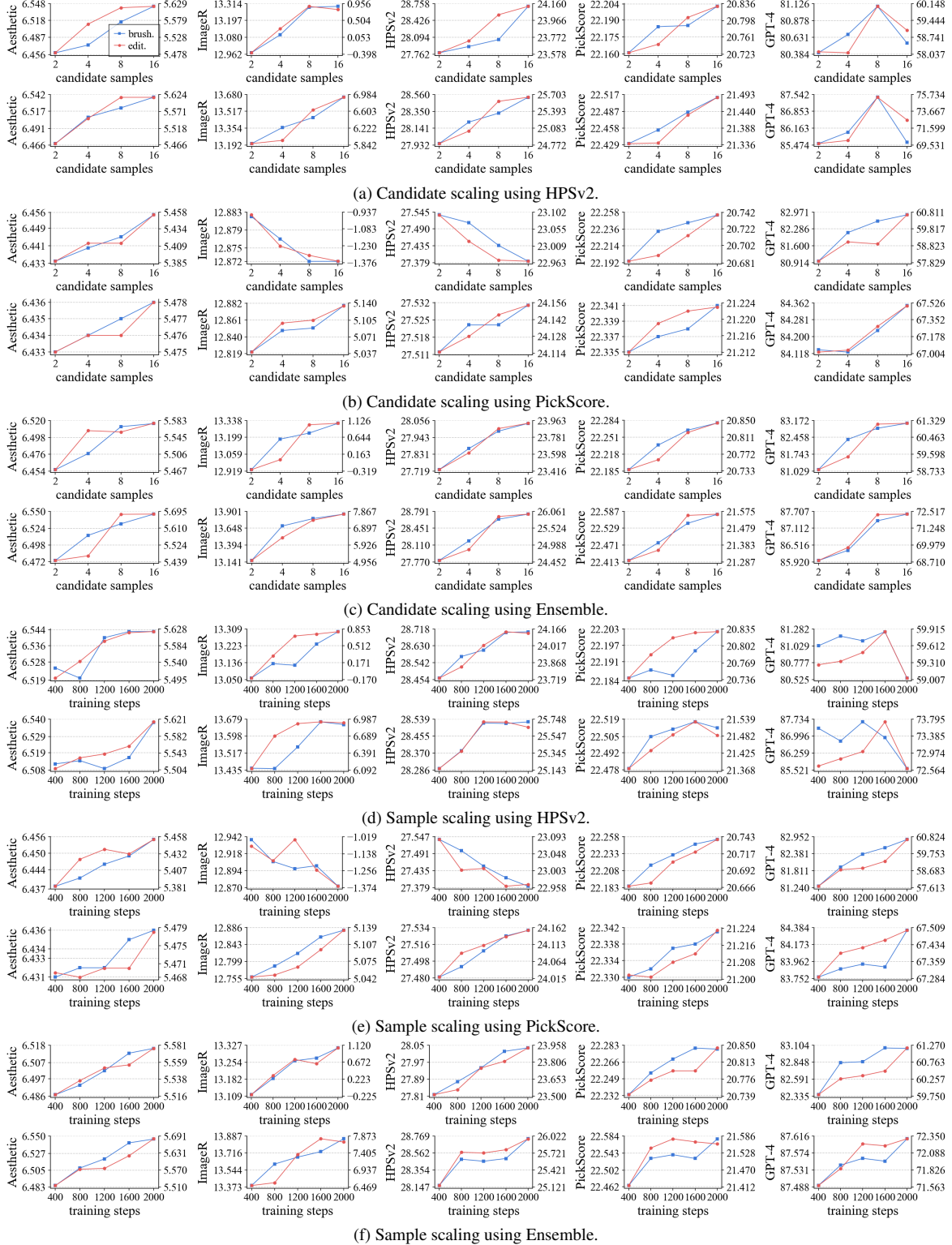


Figure 2. **Candidate scaling** (a-c) and **sample scaling** (d-f) using HPSv2, PickScore, and Ensemble. We employ Aesthetic, ImageR, HPSv2, PickScore, and GPT-4 for evaluation. The first and second row of each sub-figure is based on BrushNet and FLUX.1 Fill, respectively. We use training steps to indicate the consumed samples to align the scaling across models (their batch-sizes are different).

prompt for GPT-4 is: *You are an expert in analysis of image inpainting. Please evaluate the image inpainting result based on three criteria: Aesthetic Quality (0–40 points)—visual appeal in color harmony, composition, and style coherence, as well as texture realism and naturalness; Structural Coherence (0–30 points)—preservation of geometric structures and content continuity, and seamlessness at mask boundaries; Semantic Alignment (0–30 points)—faithfulness to the Text Prompt instructions and contextual consistency of added or restored content. For each criterion, provide a sub-score and a 1–2-sentence justification, then compute the total score (0–100).*

We report two other results. **Baseline:** The model’s performance prior to DPO training. **Random:** It involves training with randomly sampled preferred and dispreferred pairs. Results are reported in Table 1 and Table 2. We have the following observations and conclusions.

Some reward models are not reliable evaluators. It is believed that an accurate and robust reward model should assign high evaluation scores to models trained on its own preference dataset (i.e., the oracle reward model setting). Surprisingly, we find that CLIPScore, VQAScore, and Perception fail to meet this requirement—in Table 2, their scores can be even lower than those of the baseline or the random-pair baseline. We hypothesize that the failure of CLIPScore and Perception stems from their large-scale yet potentially coarse contrastive pre-training, and the failure of VQAScore likely arises from its simplistic, VQA-like evaluation approach. In light of this, *we exclude these models from subsequent analyses.*

Most reward models provide valid reward scores. Most reward models are capable of offering valid reward scores for preference data construction, as they outperform both the baseline and random selection across most evaluation results—especially GPT-4. Even though CLIPScore and Perception are observed to be less effective at accurately evaluating on small-scale benchmarks, they remain viable when their reward scores are incorporated into larger-scale preference training datasets. In this context, we continue to attribute VQAScore’s limitations to its simple scoring methodology.

Reward models share common biases. We find that the model trained on HPSv2-constructed data outperforms most competitors when evaluated using public reward models. Specifically, when trained using BrushNet, it ranks first or second in 4 out of 12 evaluations; when trained using FLUX.1 Fill, it ranks first or second in 9 out of 12 evaluations. This pattern aligns with GPT-4’s results when using FLUX.1 Fill but diverges when using BrushNet—under the latter condition, the model is largely outperformed by PickScore. We posit that HPSv2 and many other models may share some common biases, which can potentially lead to reward hacking [48].

Ensemble is an accurate and robust reward model. It shows that Ensemble ranks first or second in 11 out of 12 public model evaluations when using BrushNet, and 7 out of 12 when using FLUX.1 Fill. Besides, Ensemble ranks first or second in 3 out of 4 GPT-4’s evaluations across both baseline models, demonstrating its robustness in constructing effective preference data. We hypothesize that its versatility arises from the bias of reward models being weakened in Ensemble.

5. How Scalable are Preference Data?

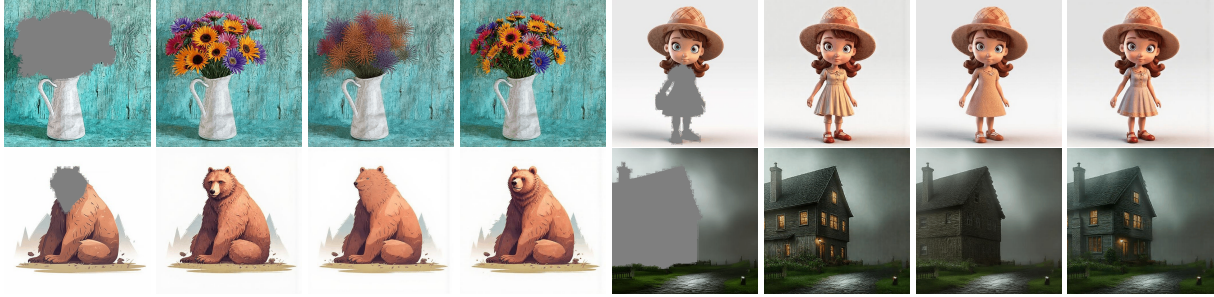
The results in section 4 have shown that HPSv2, PickScore, and Ensemble are the most effective reward models for preference data construction. Building on this finding, we conduct an investigation into the scalability of preference data using these reward models. Specifically, we explore along two dimensions: (1) **Candidate scaling.** As the number of candidate samples generated from different random seeds increases, their diversity expands. Larger candidate diversity widens the quality gap between the highest- and lowest-scoring samples, making the constructed preference pairs more informative. (2) **Sample scaling.** A larger dataset enables the model to capture nuanced patterns more comprehensively, leading to deeper learning of preferences. Based on the insights in section 4, we select Aesthetic, ImageR, HPSv2, PickScore, and GPT-4 as the evaluation models. To enable the model to achieve optimal performance, we conduct a search over two typical hyper-parameters— β and learning rate (see details in the Appendix), before the scaling experiments. For each experiment, we tune one scaling dimension and fix the other dimension. The results are reported in Figure 2. We have the following results and discoveries.

Consistent scaling trends across models and benchmarks. First, we observe that data scaling demonstrates robust trends regardless of the model used—BrushNet and FLUX.1 Fill, in the first and second rows of each sub-figure, respectively. Second, we find that similar scaling trends emerge when evaluating on different benchmarks, as evidenced by the comparable patterns of the two lines within each sub-figure. These findings indicate that the observed scaling behavior is robust and generalizable. However, we also observe some inconsistent phenomena: when using PickScore as the reward model, ImageR/HPSv2 exhibit opposite trends on BrushNet and FLUX.1 Fill. This issue is caused by the characteristics of both reward models and baseline models, as analyzed in section 6.

Reward hacking from HPSv2 undermines training. When evaluated by Aesthetic, ImageR, HPSv2, and PickScore, using HPSv2 as the reward model shows benefits from both candidate scaling and sample scaling. However, its GPT-4 results deteriorate significantly in the later stages of scaling. This observation aligns with our finding in section 4, where HPSv2 achieves good results under public model evaluations but sometimes loses to others when as-



(a) Examples from models trained using **BrushNet**.



(b) Examples from models trained using **FLUX.1 Fill**.

Figure 3. **Bias studies.** In each sub-figure, the four images (from left to right) display: the *masked image*, followed by inpainting results from models trained using *HPSv2*, *PickScore*, and *Ensemble*. We omit text prompts for brevity. Zoom in to see details. Find more examples in the Appendix.



(a) Examples from models trained using **BrushNet**.



(b) Examples from models trained using **FLUX.1 Fill**.

Figure 4. **Qualitative results of ablations.** In each sub-figure, the three images (from left to right) display: the *masked image*, followed by inpainting results from *baseline models* and *baseline models + preference alignment using Ensemble*. We omit text prompts for brevity. Zoom in to see details.

essed by GPT-4. We hypothesize that this degradation stems from some shared common biases among these reward models.

Ensemble offers robust data scaling by resisting hacking. Although *PickScore* demonstrates good scaling behavior, its performance remains sub-optimal. In contrast, the *Ensemble* approach achieves the best results across benchmarks, model structures, evaluation models, and scaling dimensions. This is likely because *Ensemble* averages the preference choices of different reward models, which eliminates the biases of the employed reward models and improves its resistance to the hacking.

6. How does Reward Hacking Happen?

We identify potential biases in reward models that may lead to reward hacking, as discussed in [section 4](#) and [section 5](#). In this section, we delve deeper into exploring these intriguing biases—examining their nature and how they make reward hacking happen. To investigate it, we sample inpainting examples in [Figure 3](#) and [Figure 4](#). We report the following findings and insights.

Reward models exhibit biases in brightness, composition, and color scheme. As evidenced by the results from *HPSv2* and *PickScore*—the second and third images in each sub-figure of [Figure 3](#) respectively, we observe notable biases

Table 3. Ablation studies on a new dataset of *I Dream My Painting* [14].

inpainting model	CLIPScore	Aesthetic	ImageR	PickScore	HPSv2	VQAScore	UnifiedR	Perception	HPSv3	GPT-4
BrushNet	24.849	5.923	-0.246	20.550	19.749	8.503	2.317	27.317	-0.551	72.669
BruPA (ours)	25.460	6.111	2.152	20.735	21.086	8.653	2.463	28.294	1.265	73.739
FLUX.1 Fill	24.194	6.017	0.544	20.855	20.203	8.667	2.476	26.627	0.547	76.391
FluPA (ours)	25.500	6.448	5.961	21.407	23.770	9.031	2.784	28.868	5.023	79.255

Bold values denote the best results.

Table 4. Comparisons of state-of-the-art image inpainting models on BrushBench and EditBench.

inpainting model	CLIPScore		Aesthetic		ImageR		PickScore		HPSv2		VQAScore		UnifiedR		Perception		HPSv3		GPT-4	
	Brush.	Edit.	Brush.	Edit.	Brush.	Edit.	Brush.	Edit.	Brush.	Edit.	Brush.	Edit.	Brush.	Edit.	Brush.	Edit.	Brush.	Edit.	Brush.	Edit.
SDI	26.304	26.526	6.368	5.377	12.026	-1.100	22.105	20.791	27.079	23.203	8.981	6.923	3.268	2.069	26.190	25.382	5.320	0.849	79.004	60.751
CNI	26.341	26.972	6.305	5.382	11.421	-1.044	21.953	20.874	26.633	23.076	8.890	6.906	3.218	2.125	26.150	25.894	4.546	0.894	74.173	63.921
BLD	26.337	27.666	6.262	5.372	11.161	0.563	21.901	20.980	26.723	23.839	8.852	7.467	3.202	2.228	26.128	<u>27.093</u>	4.559	1.114	71.794	62.690
PowerPaint	26.265	27.291	6.312	5.448	11.771	0.720	22.089	20.912	27.065	23.347	8.931	7.238	3.271	2.219	26.123	26.264	5.112	1.068	78.241	63.092
PrefPaint	26.268	25.569	6.377	5.296	11.798	-3.023	22.125	20.666	26.855	22.241	8.925	6.226	3.271	1.951	26.116	24.264	5.208	-0.336	80.327	60.815
StrDiffusion	23.872	21.398	5.330	4.405	-0.063	-16.282	20.342	19.147	21.431	16.616	7.281	3.662	2.417	1.236	23.381	20.102	-2.243	-7.131	34.255	25.200
HD-Painter	26.367	26.934	6.480	<u>6.640</u>	12.913	0.046	22.314	21.016	27.931	23.951	9.019	6.682	3.349	2.136	26.214	25.721	6.224	1.983	<u>85.016</u>	<u>69.087</u>
ASUKA	24.387	20.842	6.294	5.078	5.208	-14.110	21.601	19.603	25.285	18.702	7.681	3.631	2.862	1.282	23.959	19.017	3.556	-3.506	75.140	58.686
BrushNet	26.415	27.337	6.425	5.392	12.717	-1.296	22.133	20.616	27.509	23.076	9.060	6.770	3.303	2.100	<u>26.290</u>	26.410	5.749	0.403	79.391	57.046
BruPA (ours)	26.547	<u>27.694</u>	<u>6.516</u>	5.577	<u>13.315</u>	10.463	22.279	20.844	<u>28.037</u>	23.933	<u>9.093</u>	7.043	<u>3.371</u>	2.193	26.390	26.881	<u>6.276</u>	1.398	83.054	61.186
FLUX.1 Fill	26.244	27.103	6.429	5.458	12.760	4.910	<u>22.327</u>	<u>21.211</u>	27.476	<u>24.076</u>	9.081	<u>8.021</u>	3.360	<u>2.485</u>	25.945	26.834	6.055	<u>2.470</u>	83.935	66.979
FluPA (ours)	<u>26.436</u>	27.813	6.546	5.681	13.859	<u>7.707</u>	22.577	21.559	28.735	25.972	9.152	8.434	3.457	2.649	26.096	27.617	7.000	4.230	87.609	72.307

Bold values denote the best results. Underlined values denote the second-best results. All methods are evaluated using official implementations with blending [23].

in their preferences. HPSv2 tends to favor images with bright lighting, complex composition with rich details, and vivid colors. In contrast, PickScore shows a preference for dim lighting, simple composition with few details, and muted colors. We also make an attempt to leverage GPT-4 for evaluating generation biases quantitatively. We report the results on BrushBench in Table 5. The quantitative results well validate our analyses that HPSv2 favors images with bright lighting, complex composition, and vivid colors; PickScore shows the opposite tendency; and our Ensemble falls squarely between the two.

Table 5. Quantitative results of biases evaluated by GPT-4.

model	reward model	brightness	composition	color
BrushNet	HPSv2	79.221	82.979	81.267
	Ensemble	<u>78.180</u>	<u>80.922</u>	<u>78.513</u>
	PickScore	73.545	75.019	70.641
FLUX.1 Fill	HPSv2	76.617	74.547	70.978
	Ensemble	<u>76.412</u>	<u>74.057</u>	<u>70.496</u>
	PickScore	76.124	73.512	69.824

Biases in reward models affect different baseline models in distinct ways. Although each reward model has

its own inherent biases, we find that their influence varies across baseline models. For instance, BrushNet trained using HPSv2 produces inpainting outputs characterized by excessively bright lighting, overly intricate details, and unnaturally vivid colors—they seem to deviate from human aesthetic preferences. In contrast, FLUX.1 Fill trained using HPSv2 generates visually pleasing results. PickScore shows a similar disparity in performance. It stems from the characteristics of baseline models as shown in Figure 4: BrushNet generates vibrant images, making PickScore particularly suitable for it; while FLUX.1 Fill produces plain images, aligning with HPSv2’s property.

Ensemble shows generality and generalization by mitigating biases. Ensemble, a simple and straightforward method implemented through reward ensembling, exhibits strong versatility across models by producing balanced and aesthetically pleasing inpainting results, as shown in Figure 3 and Figure 4. It likely stems from Ensemble’s ability to mitigate biases inherent in reward models.

7. What is the Origin of the Biases?

To better understand the source of the biases identified above, we examine the training data of two representative reward models—HPSv2 and PickScore—whose biases run in opposite directions. Specifically, we sample 1,000 preference



Figure 5. Qualitative comparisons with state-of-the-art image inpainting models.

pairs (each consisting of one winning and one losing sample) from HPDv2 [70] and Pick-a-Pic [25], the datasets used to train HPSv2 and PickScore, respectively. We then prompt GPT-4 to score these images along three attributes—brightness, composition, and color—and report the results in Table 6. As expected, HPDv2 exhibits substantial gaps between its winning and losing samples across all three attributes, whereas Pick-a-Pic shows only marginal differences. These dataset characteristics offer a natural explanation for the model-level behavior observed in previous sections: HPSv2 tends to favor bright, compositionally complex, and vividly colored images, whereas PickScore exhibits the opposite tendency.

Table 6. Bias analysis on HPDv2 and Pick-a-Pic.

dataset	brightness			composition			color		
	win	loss	win-lose	win	loss	win-lose	win	loss	win-lose
HPDv2	40.641	39.236	1.405	45.208	41.560	3.648	42.340	38.269	4.071
Pick-a-Pic	42.421	42.415	0.006	46.144	45.899	0.245	43.943	44.137	-0.194

8. Ablation Studies and Comparisons with State-of-the-Art

We name our methods **BruPA** and **FluPA**—BrushNet and FLUX.1 Fill with Ensemble-based preference alignment. We compare them with state-of-the-art image inpainting

models. Specifically, the following methods are compared (they are introduced in section 2): SDI [52], CNI [78], BLD [2], PowerPaint [80], BrushNet [23], PrefPaint [35], StrDiffusion [33], FLUX.1 Fill [8], HD-Painter [47], and ASUKA [67], where *BrushNet* and *FLUX.1 Fill* are also the baseline models for ablation studies.

Table 7. Details of GPT-4 evaluations.

inpainting model	overall	aesthetics	structure	semantics
BrushNet	79.391	30.301	24.035	25.055
BruPA	83.054	33.516	24.069	25.469
FLUX.1 Fill	83.935	32.617	24.997	26.321
FluPA	87.609	35.100	25.627	26.883

Ablation studies on preference alignment. We report quantitative and qualitative ablation studies, before and after preference alignment training, in Table 4 and Figure 4, respectively. After preference alignment using Ensemble, our method significantly surpasses the baseline models by achieving much better results and yielding visually appealing results. We also report the details of GPT-4 evaluation in Table 7. According to GPT-4 on each sub-dimension, preference alignment consistently improves image quality across all aspects—esthetic appeal, structure accuracy, and semantic alignment. We further conduct ablation studies on a new

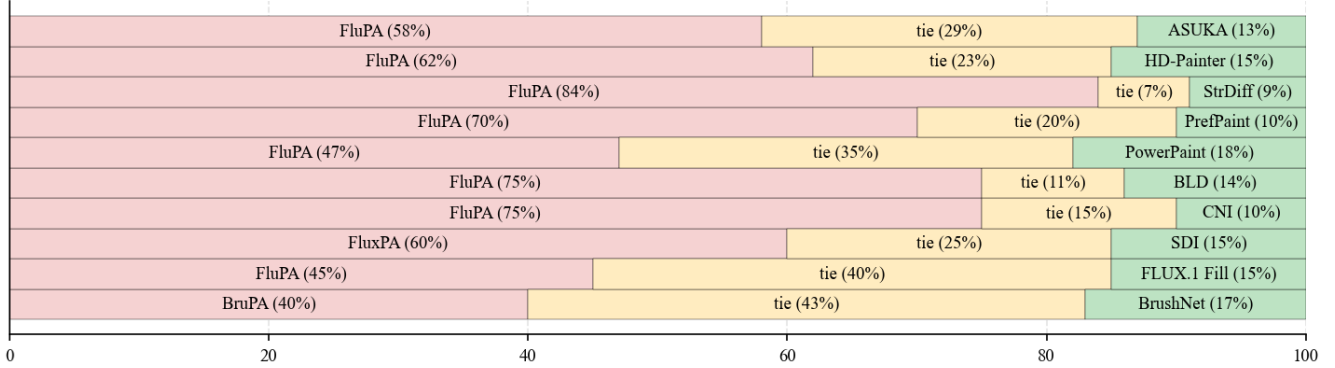


Figure 6. **User studies.** We compare each pair of models by randomly sampling 100 pairs from their inpainting results. We invite 30 volunteers to participate in a blind assessment to determine which one is better (“A win”, “B win”, or “tie”) based on their preferences. We report the **winning rates**.

Table 8. Evaluation by GPT-4 and Qwen3-VL

inpainting model	GPT-4		Qwen3-VL	
	Brush.	Edit.	Brush.	Edit.
SDI	79.004 ± 0.203	63.921 ± 0.410	90.323 ± 0.245	88.300 ± 0.310
CNI	74.173 ± 0.817	60.751 ± 0.590	88.101 ± 0.277	85.519 ± 0.337
BLD	71.794 ± 0.657	62.690 ± 0.736	85.719 ± 0.461	86.886 ± 0.336
PowerPaint	78.241 ± 0.912	63.092 ± 0.738	89.763 ± 0.250	85.682 ± 0.425
PrefPaint	80.327 ± 0.293	60.815 ± 0.392	91.249 ± 0.220	83.269 ± 0.449
StrDiffusion	34.255 ± 0.159	25.200 ± 0.236	49.560 ± 0.394	40.867 ± 0.336
HD-Painter	<u>85.016</u> ± 0.626	<u>69.089</u> ± 0.628	92.361 ± 0.026	87.389 ± 0.325
ASUKA	75.140 ± 1.022	58.686 ± 0.477	84.597 ± 0.458	73.614 ± 0.980
BrushNet	79.391 ± 0.375	57.046 ± 1.151	89.930 ± 0.396	85.064 ± 0.450
BruPA (ours)	83.054 ± 0.886	61.081 ± 0.764	92.255 ± 0.163	<u>88.686</u> ± 0.248
FLUX.1 Fill	83.935 ± 0.414	67.465 ± 0.463	<u>92.752</u> ± 0.145	88.649 ± 0.306
FluPA (ours)	87.609 ± 0.291	72.307 ± 0.560	94.501 ± 0.154	91.603 ± 0.220

dataset, which are reported in Table 3. It also confirms that our improvement is generalizable across data distributions.

Comparisons with state-of-the-art. Table 4 reports the results. Our BruPA and FluPA set new state-of-the-art results, attaining the best scores on all evaluations and the second-best scores in nearly half of the cases. Notably, even on coarser metrics—CLIPScore, VQAScore, and Perception (analyzed in section 4)—our methods still outperform competitors. Besides, BruPA and FluPA significantly outperform BrushNet and FLUX.1 Fill, i.e., the baselines before applying preference alignment. The qualitative results are reported in Figure 5, and our models generate images with better aesthetics.

Effectiveness of GPT-4. To validate the effectiveness of GPT-4, we conduct user studies. All participants were informed of the purpose and procedure of the user study and provided informed consent before participation. The study

collected only anonymized preference judgments and did not collect personally identifiable information. We randomly selected 500 inpainting pairs and invited volunteers to judge which result is better. Our human raters were drawn completely at random from a large and diverse volunteer pool. This random selection ensures that the evaluation is representative. To quantify agreement, we compute the alignment accuracy between the reward models and human raters, defined as the average proportion of cases in which both the raters and the model prefer the same result. In our evaluation, GPT-4 achieves 86% accuracy; HPSv2: 82%, PickScore: 80%, ImageReward: 77%, and Aesthetic: 80%. To further evaluate the results, we include an open-source vision-language foundation model—Qwen3-VL [49]—for evaluation. The results with means and standard deviations are reported in Table 8. Evaluation results of GPT-4 and Qwen3-VL are broadly stable, with our BruPA and FluPA delivering consistently re-

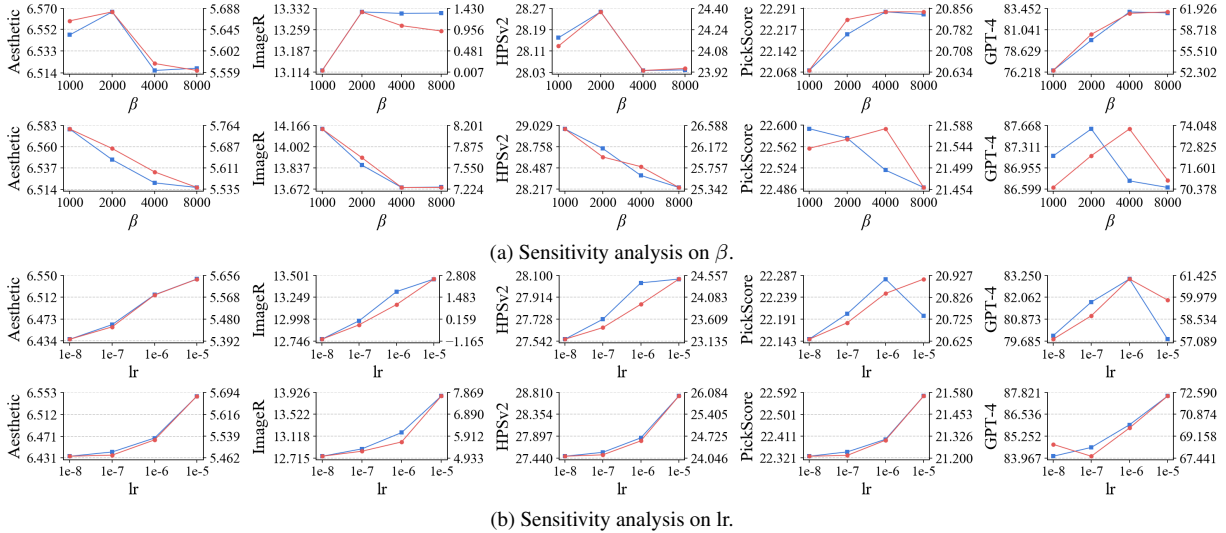


Figure 7. Searches of β , i.e., sub-figure (a), and learning rate (lr), i.e., sub-figure (b). The first and second row of each sub-figure is based on **BrushNet** and **FLUX.1 Fill**, respectively.

markable performance gains. For completeness, we also report the Qwen3-VL counterparts of Table 5 and Table 7 in Table 9 and Table 10, respectively. The conclusions remain highly consistent across different vision-language foundation models.

To eliminate the potential biases in our design of prompts, we provide more results on the weights of the criteria—*aesthetic quality*, *structural coherence*, and *semantic alignment*—in Table 11. Our BruPA and FluPA consistently outperform the baseline models by a large margin, showing the significant and robust improvement of our method in GPT-4 evaluations.

Analysis of Hyper-Parameters. We conduct hyper-parameter searches for Ensemble, as shown in Figure 7. For Ensemble, we finally adopt a learning rate of $1e-6$, and set $\beta = 4000$ for BrushNet; while using a learning rate of $1e-5$ and setting $\beta = 2000$ for FLUX.1 Fill. For HPSv2, we use a learning rate of $1e-5$ with $\beta = 4000$ for BrushNet; and a learning rate of $1e-6$ with $\beta = 8000$ for FLUX.1 Fill. For PickScore, we set the learning rate to $1e-7$ and use $\beta = 2000$ for both BrushNet and FLUX.1 Fill.

We also find that fine-tuning these hyper-parameters is not critical. Even when using fixed moderate values ($\beta = 4000$ and $lr = 1e-6$, as suggested by [61]) across all experiments, our method still far exceeds the baseline w/o DPO: BruPA on BrushBench (83.133 vs. 79.391), BruPA on EditBench (72.442 vs. 57.046), FluPA on BrushBench (86.337 vs. 83.935), FluPA on EditBench (77.908 vs. 66.979). The new results remain the SOTA by outperforming previous best methods: BrushBench (86.337 vs. 85.016) and EditBench (77.908 vs. 69.087). Besides, Ensemble is less sensitive to hyper-parameter variations than single reward models like HPSv2 and PickScore. We hypothesize that this robustness

Table 9. Quantitative results of biases evaluated by Qwen3-VL.

model	reward model	brightness	composition	color
BrushNet	HPSv2	83.843	88.310	85.565
	Ensemble	<u>83.284</u>	<u>88.180</u>	<u>84.644</u>
	PickScore	82.615	86.530	82.516
FLUX.1 Fill	HPSv2	82.750	85.832	81.695
	Ensemble	<u>82.527</u>	<u>85.611</u>	<u>81.454</u>
	PickScore	82.508	85.481	81.389

Table 10. Details of Qwen3-VL evaluations.

inpainting model	overall	aesthetics	structure	semantics
BrushNet	89.930	35.141	27.395	27.393
BruPA	92.255	36.032	28.018	28.204
FLUX.1 Fill	92.752	36.244	28.080	28.426
FluPA	94.501	36.972	28.477	29.052

arises because the Ensemble integrates different reward models, thereby mitigating the sensitivity inherent to any individual reward model.

Table 11. GPT-4 evaluation results with different weight combinations: [aesthetic quality]-[structural coherence]-[semantic alignment]. “auto” represents the weight is determined by GPT-4 itself.

inpainting model	40-30-30	30-40-30	30-30-40	33-33-33	auto
BrushNet	79.391	78.423	77.937	78.169	77.388
BruPA	83.054	82.538	82.388	82.226	81.036
FLUX.1 Fill	83.935	83.746	83.229	83.217	81.649
FluPA	87.609	87.559	87.368	87.243	85.309

Compute Costs of Each Reward Model. We report the

Table 12. Compute cost for giving score to a single sample.

reward model	CLIPScore	Aesthetic	ImageR	PickScore	HPSv2	VQAScore	UnifiedR	Perception	HPSv3
cost (seconds)	0.154	0.048	0.0759	0.0319	0.219	0.288	3.051	0.155	0.379



(a) Examples from models trained using **BrushNet**.



(b) Examples from models trained using **FLUX.1 Fill**.

Figure 8. **Different Ensemble variants.** In each sub-figure, the four images (from left to right) display: the *masked image*, followed by inpainting results from models trained using *Ensemble (vanilla)*, *Ensemble (w/o VQAScore)*, and *Ensemble (Linear)*. We omit text prompts for brevity. Zoom in to see details.

compute cost of each reward model for giving a score to a single sample in Table 12. Note that our Ensemble method only introduces additional cost for scoring samples and constructing preference pairs; the cost for training remains the same as in standard methods.

User studies. As shown in Figure 6, our models align with human preferences better.

9. Stronger Ensemble Variants

We have identified biases across reward models and proposed a new reward model, **Ensemble**, to mitigate reward hacking. In this section, we further explore how to push the limit of **Ensemble**. To this end, we introduce three complementary strategies: filtering out weaker reward models, weighted ensembling, and calibrated ensembling.

Removing the weaker reward models. As discussed in section 4, we find that VQAScore is neither a reliable evaluator nor an effective reward signal provider. Therefore, we conduct a new experiment by removing this weak reward model from **Ensemble**. The quantitative results on BrushBench are reported in Table 13 and the qualitative results are

reported in Figure 8. We observe a significant improvement in the GPT-4 evaluation scores of BruPA and FluPA after excluding VQAScore. This result preliminarily suggests that removing weaker reward models, although sacrificing the diversity of reward signals, can further enhance the results of preference alignment. There seems to be a trade-off between the diversity and effectiveness of reward signals when weaker reward models are present.

Weighted Ensemble. We find that assigning different weights to reward models when constructing ensemble scores significantly affects the performance. We report the results of two new variants—*Linear Weighted Ensemble* (named **BruPA (linear)** and **FluPA (linear)**), and *Softmax Weighted Ensemble* (named **BruPA (softmax)** and **FluPA (softmax)**)—in Table 14 and Figure 8. In **BruPA (vanilla)** and **FluPA (vanilla)**, each reward model is given equal weight. In comparison, in BruPA (linear) and FluPA (linear), each reward model is weighted by its corresponding GPT-4 score (from Table 1 and Table 2), thereby granting greater influence to higher-performing models. The BruPA (softmax) and FluPA (softmax) further normalize these weights via a

Table 13. Comparisons of different Ensemble variants on removing the weaker reward models.

inpainting model	CLIPScore	Aesthetic	ImageR	PickScore	HPSv2	VQAScore	UnifiedR	Perception	HPSv3	GPT-4
BruPA	26.547	6.516	13.315	22.279	28.037	9.093	3.371	26.390	6.276	83.054
BruPA w/o VQAScore	26.555	6.524	13.337	22.278	28.055	9.082	3.362	26.385	6.306	83.659
FluPA	26.436	6.546	13.859	22.577	28.735	9.152	3.457	26.096	7.000	87.609
FluPA w/o VQAScore	26.438	6.576	14.017	22.605	28.747	9.186	3.466	26.113	7.068	88.972

Table 14. Comparisons of different Ensemble variants with different weights applied to reward models.

variant	CLIPScore	Aesthetic	ImageR	PickScore	HPSv2	VQAScore	UnifiedR	Perception	HPSv3	GPT-4
BruPA	26.547	<u>6.516</u>	<u>13.315</u>	22.279	28.037	<u>9.093</u>	<u>3.371</u>	26.390	6.276	83.054
BruPA (linear)	<u>26.568</u>	6.521	13.342	<u>22.274</u>	<u>28.050</u>	9.098	3.372	<u>26.400</u>	<u>6.288</u>	83.479
BruPA (softmax)	26.573	<u>6.516</u>	13.136	22.265	28.073	9.092	3.359	26.409	6.310	83.136
FluPA	<u>26.436</u>	6.546	<u>13.859</u>	<u>22.577</u>	<u>28.735</u>	9.152	3.457	<u>26.096</u>	<u>7.000</u>	87.609
FluPA (linear)	26.513	6.556	14.030	22.605	28.815	9.172	<u>3.452</u>	26.171	7.136	89.190
FluPA (softmax)	26.434	<u>6.553</u>	13.834	22.538	28.609	<u>9.166</u>	3.443	26.080	6.984	<u>88.145</u>

Table 15. Comparisons of different Ensemble variants with different training objectives.

variant	CLIPScore	Aesthetic	ImageR	PickScore	HPSv2	VQAScore	UnifiedR	Perception	HPSv3	GPT-4
BruPA	<u>26.547</u>	<u>6.516</u>	13.315	22.279	28.037	9.093	3.371	26.390	6.276	83.054
BruPA (CaPO)	26.567	6.522	13.269	<u>22.286</u>	27.962	<u>9.084</u>	3.350	<u>26.401</u>	6.242	<u>83.659</u>
BruPA (CaEN)	26.537	6.515	<u>13.288</u>	22.293	<u>28.032</u>	9.062	<u>3.358</u>	26.410	<u>6.259</u>	83.717
FluPA	26.436	<u>6.546</u>	<u>13.859</u>	<u>22.577</u>	28.735	<u>9.152</u>	<u>3.457</u>	<u>26.096</u>	7.000	87.609
FluPA (CaPO)	26.398	6.498	13.773	22.559	28.398	9.161	3.433	26.075	6.808	<u>88.499</u>
FluPA (CaEN)	<u>26.421</u>	6.557	13.934	22.616	<u>28.642</u>	9.161	3.474	26.114	<u>6.993</u>	88.541

softmax transformation. Based on GPT-4 evaluations, both linear and softmax variants outperform the vanilla Ensemble approach. However, these weighting strategies remain overly simple and may further exacerbate reward hacking.

Ensemble as a calibrated reward. One core difficulty in multi-reward preference alignment lies in the inconsistency across the reward distributions. CaPO [27] addresses this challenge by approximating the advantage of sample x_i using the average pairwise win rate between x_i and x_j in the batch $\{\mathbf{x}_i\}_{i=1}^N$ sampled from the reference policy $p_{\text{ref}}(\cdot|\mathbf{c})$ under the conditions \mathbf{c} for a given reward model R :

$$R_{\text{ca}}(\mathbf{x}_i, \mathbf{c}) = \frac{1}{N-1} \sum_{j \neq i} \sigma(R(\mathbf{x}_i, \mathbf{c}) - R(\mathbf{x}_j, \mathbf{c})). \quad (5)$$

For an ensemble of L reward models, the calibrated reward is given by

$$R_{\text{ca}}(\mathbf{x}, \mathbf{c}) = \frac{1}{L} \sum_{j=1}^L R_{\text{ca}}^{(j)}(\mathbf{x}, \mathbf{c}). \quad (6)$$

Even though Equation 5 and Equation 6 align the scales of different reward models, they ignore the differences in variance. To this end, we revisit the **Ensemble** and reformulate it as

$$R_{\text{En}}(\mathbf{x}_i, \mathbf{c}) = \frac{1}{N-1} \sum_{j \neq i} \mathbf{1}\{R(\mathbf{x}_i, \mathbf{c}) > R(\mathbf{x}_j, \mathbf{c})\}, \quad (7)$$

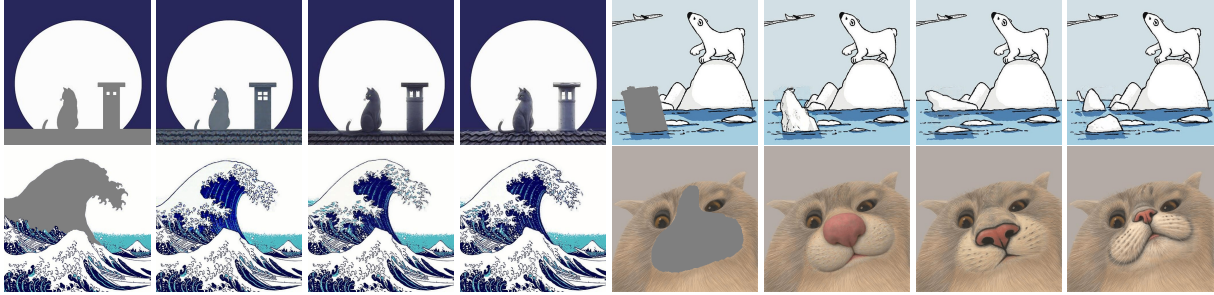
where $\mathbf{1}\{\cdot\}$ denotes the indicator function. We further replace the calibrated reward in CaPO with Equation 7, which yields the CaEN loss:

$$R_{\text{En}}(\mathbf{x}, \mathbf{c}) = \frac{1}{L} \sum_{j=1}^L R_{\text{En}}^{(j)}(\mathbf{x}, \mathbf{c}). \quad (8)$$

Equation 7 and Equation 8 not only account for scale alignment, but also eliminate the influence of variance differences.



(a) Examples from models trained using **BrushNet**.



(b) Examples from models trained using **FLUX.1 Fill**.

Figure 9. **Qualitative results.** In each sub-figure, the four images (from left to right) display: the *masked image*, followed by inpainting results from models trained using *Ensemble (vanilla)*, *CaPO*, and *CaEN*. We omit text prompts for brevity. Zoom in to see details. Find more examples in the Appendix.

Following CaPO, we obtain the CaEN objective:

$$\mathcal{L}_{\text{CaEN}}(\theta) = \mathbb{E}_{t, \epsilon^w, \epsilon^l} \left[\left(R_{\text{En}}(\mathbf{x}^w, \mathbf{c}) - R_{\text{En}}(\mathbf{x}^l, \mathbf{c}) - (-\beta((\mathcal{L}_\theta^w - \mathcal{L}_{\text{ref}}^w) - (\mathcal{L}_\theta^l - \mathcal{L}_{\text{ref}}^l))) \right)^2 \right], \quad (9)$$

where we assign different noises $\epsilon^w, \epsilon^l \sim \mathcal{N}(0, I)$ to $(\mathcal{L}_\theta^w, \mathcal{L}_{\text{ref}}^w)$ and $(\mathcal{L}_\theta^l, \mathcal{L}_{\text{ref}}^l)$, following CaPO. We train FLUX.1 fill using a learning rate of 1e-5 and choose β by sweeping over $\{30, 50, 100\}$ for both CaPO and CaEN. For BrushNet, we use a learning rate of 1e-6 and choose β by sweeping over $\{300, 500, 1000\}$ for both CaPO and CaEN, and we report the comparison among vanilla Ensemble, CaPO and CaEN in Table 15. Similar to the observations in section 4, we find that models trained on vanilla Ensemble-constructed data, including both BruPA and FluPA, outperform those trained on CaPO-constructed data when evaluated by public reward models but fail under GPT-4 evaluation. On top of this, we posit that reward hacking still undermines Ensemble while CaPO and CaEN further mitigate the hacking. To further understand the potential biases in Ensemble, we sample inpainting examples and present them in Figure 9 and the appendix. Empirically, we find that CaEN amplifies the biases shared across reward models, as discussed in section 4. To offset these biases, we assign higher weights to CLIPScore and Perception. Besides, compared with CaPO, CaEN attains the best results in 8 out of 10 evaluations and

the second-best results in more than half of the cases. Both qualitative and quantitative results consistently demonstrate that both CaPO and CaEN mitigate the biases inherent in the vanilla Ensemble, with CaEN exhibiting better performance.

10. Application to Object Removal

In this section, we evaluate preference alignment with the proposed method on the task of object removal.

10.1. Experiment Setup

Training details. We generate preference data on the high-quality object removal dataset RORem [29]. Specifically, we generate 16 candidates for each image-mask pair and leave the text prompt empty. We train BruPA and FluPA for 800 steps, following the same training recipes.

Evaluation details. We construct the test set by randomly sampling 600 image-mask pairs from RORD-Val [29]. We evaluate the efficacy of our methods using three widely adopted metrics: PSNR, CLIPScore [20], and LPIPS [79].

10.2. Comparison with the Baselines

To evaluate the efficacy of preference alignment, we report the results in Table 16. The results demonstrate that BruPA and FluPA significantly outperform their baseline models on the object-removal task. This observation suggests that our method may generalize to other image inpainting and editing tasks. We attribute this improvement to the fact that prefer-

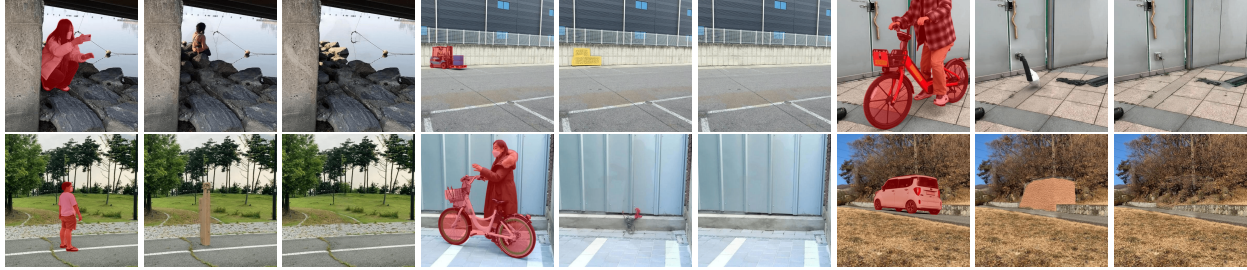


Figure 10. **Qualitative results of ablations in object removal.** In each sub-figure, the three images (from left to right) display: the *masked image*, followed by inpainting results from *baseline models* and *baseline models + preference alignment*.

Table 16. Results for object removal.

inpainting model	CLIPScore	PSNR	PSNR-BG	LPIPS \downarrow
BrushNet	87.640	0.116	43.445	0.082
BruPA	89.896	1.342	43.791	0.071
FLUX.1 Fill	92.736	3.615	43.820	0.051
FluPA	93.549	4.353	44.072	0.047

ence alignment training suppressing the model’s tendency to generate spurious or hallucinated content.

11. Conclusion and Discussion

We conduct extensive studies on image inpainting with preference alignment and obtain key insights into the effectiveness, scalability, and challenges in achieving alignment. We find that a simple ensemble method mitigates biases and achieves non-trivial results in the conference version of this work. We further generalize preference alignment from creative image inpainting to object-removal inpainting, a more challenging setting that emphasizes coherent and visually plausible background completion rather than open-ended generation. We provide a substantially more comprehensive investigation of the ensemble strategy by analyzing its limitations under reward hacking, studying weighting schemes across reward models, and examining the efficiency gains enabled by filtering out invalid reward signals. Building upon the simple ensemble method, we find it still vulnerable to reward hacking, and we therefore propose a calibrated ensemble that mitigates bias-induced hacking and establishes a new state of the art.

12. Limitations and Potential Negative Social Impacts

Our work has the following limitations. First, our work is confined to image data, and we leave the extension of these findings to video and 3D data as future work. Second, our approach relies on off-the-shelf reward models to construct

preference training data. As shown in our analysis, these reward models can exhibit biases and may induce reward hacking. While our ensemble and calibrated ensemble methods improve robustness, they may not fully eliminate this issue. Finally, our evaluation still depends partly on automatic evaluators, including vision-language model-based judges, which cannot fully replace human judgments. Researchers should also be aware of the potential negative social impacts arising from the misuse of inpainting models. For example, such models can generate highly realistic content that may be indistinguishable from real photographs.

References

- [1] Josh Achiam, Steven Adler, Sandhini Agarwal, Lama Ahmad, Ilge Akkaya, Florencia Leoni Aleman, Diogo Almeida, Janko Altschmidt, Sam Altman, Shyamal Anadkat, et al. Gpt-4 technical report. *arXiv preprint arXiv:2303.08774*, 2023. 5
- [2] Omri Avrahami, Ohad Fried, and Dani Lischinski. Blended latent diffusion. *ACM transactions on graphics*, 2023. 2, 10
- [3] Mohammad Gheshlaghi Azar, Zhaohan Daniel Guo, Bilal Piot, Remi Munos, Mark Rowland, Michal Valko, and Daniele Calandriello. A general theoretical paradigm to understand learning from human preferences. In *International Conference on Artificial Intelligence and Statistics*, 2024. 2
- [4] Yuntao Bai, Andy Jones, Kamal Ndousse, Amanda Askell, Anna Chen, Nova DasSarma, Dawn Drain, Stanislav Fort, Deep Ganguli, Tom Henighan, et al. Training a helpful and harmless assistant with reinforcement learning from human feedback. *arXiv preprint arXiv:2204.05862*, 2022. 3
- [5] Marcelo Bertalmio, Guillermo Sapiro, Vincent Caselles, and Coloma Ballester. Image inpainting. In *Proceedings of the 27th annual conference on Computer graphics and interactive techniques*, 2000. 1, 2
- [6] Kevin Black, Michael Janner, Yilun Du, Ilya Kostrikov, and Sergey Levine. Training diffusion models with reinforcement learning. *arXiv preprint arXiv:2305.13301*, 2023. 1, 3
- [7] BlackForestLabs. Flux.1-dev. <https://huggingface.co/black-forest-labs/FLUX.1-dev>, 2024. Accessed: 2025-07-12. 2
- [8] BlackForestLabs. Flux.1-fill-dev. <https://huggingface.co/black-forest-labs/FLUX.1-Fill-dev>, 2024. Accessed: 2025-07-12. 1, 3, 10

- [9] Daniel Bolya, Po-Yao Huang, Peize Sun, Jang Hyun Cho, Andrea Madotto, Chen Wei, Tengyu Ma, Jiale Zhi, Jathushan Rajasegaran, Hanoona Rasheed, et al. Perception encoder: The best visual embeddings are not at the output of the network. *arXiv preprint arXiv:2504.13181*, 2025. 5
- [10] Tim Brooks, Aleksander Holynski, and Alexei A Efros. Instructpix2pix: Learning to follow image editing instructions. In *IEEE/CVF Conference on Computer Vision and Pattern Recognition*, 2023. 3
- [11] Qihua Chen, Yue Ma, Hongfa Wang, Junkun Yuan, Wenzhe Zhao, Qi Tian, Hongmei Wang, Shaobo Min, Qifeng Chen, and Wei Liu. Follow-your-canvas: Higher-resolution video outpainting with extensive content generation. *arXiv preprint arXiv:2409.01055*, 2024. 2
- [12] Patrick Esser, Sumith Kulal, Andreas Blattmann, Rahim Entezari, Jonas Müller, Harry Saini, Yam Levi, Dominik Lorenz, Axel Sauer, Frederic Boesel, et al. Scaling rectified flow transformers for high-resolution image synthesis. In *International conference on machine learning*, 2024. 2, 3
- [13] Ying Fan, Olivia Watkins, Yuqing Du, Hao Liu, Moonkyung Ryu, Craig Boutilier, Pieter Abbeel, Mohammad Ghavamzadeh, Kangwook Lee, and Kimin Lee. Dpok: Reinforcement learning for fine-tuning text-to-image diffusion models. *Advances in Neural Information Processing Systems*, 2023. 1, 3
- [14] Nicola Fanelli, Gennaro Vessio, and Giovanna Castellano. I dream my painting: Connecting mllms and diffusion models via prompt generation for text-guided multi-mask inpainting. In *IEEE/CVF Winter Conference on Applications of Computer Vision*, 2025. 9
- [15] Kunyu Feng, Yue Ma, Bingyuan Wang, Chenyang Qi, Haozhe Chen, Qifeng Chen, and Zeyu Wang. Dit4edit: Diffusion transformer for image editing. In *Proceedings of the AAAI Conference on Artificial Intelligence*, pages 2969–2977, 2025. 2
- [16] Yu Gao, Lixue Gong, Qiushan Guo, Xiaoxia Hou, Zhichao Lai, Fanshi Li, Liang Li, Xiaochen Lian, Chao Liao, Liyang Liu, et al. Seedream 3.0 technical report. *arXiv preprint arXiv:2504.11346*, 2025. 3
- [17] Yu Gao, Haoyuan Guo, Tuyen Hoang, Weilin Huang, Lu Jiang, Fangyuan Kong, Huixia Li, Jiashi Li, Liang Li, Xiaojie Li, et al. Seedance 1.0: Exploring the boundaries of video generation models. *arXiv preprint arXiv:2506.09113*, 2025. 3
- [18] Daya Guo, Dejian Yang, Haowei Zhang, Junxiao Song, Ruoyu Zhang, Runxin Xu, Qihao Zhu, Shirong Ma, Peiyi Wang, Xiao Bi, et al. Deepseek-r1: Incentivizing reasoning capability in llms via reinforcement learning. *arXiv preprint arXiv:2501.12948*, 2025. 3
- [19] Amir Hertz, Ron Mokady, Jay Tenenbaum, Kfir Aberman, Yael Pritch, and Daniel Cohen-Or. Prompt-to-prompt image editing with cross attention control. *arXiv preprint arXiv:2208.01626*, 2022. 3
- [20] Jack Hessel, Ari Holtzman, Maxwell Forbes, Ronan Le Bras, and Yejin Choi. Clipscore: A reference-free evaluation metric for image captioning. *arXiv preprint arXiv:2104.08718*, 2021. 5, 15
- [21] Jonathan Ho, Ajay Jain, and Pieter Abbeel. Denoising diffusion probabilistic models. *Advances in neural information processing systems*, 2020. 1, 2, 3
- [22] Zijing Hu, Junkun Yuan, Kairong Han, Yunze Tong, Shengyu Zhang, Fei Wu, and Kun Kuang. Reinforcement learning in generative multimodal ai: A survey. *Authorea Preprints*, 2026. 3
- [23] Xuan Ju, Xian Liu, Xintao Wang, Yuxuan Bian, Ying Shan, and Qiang Xu. Brushnet: A plug-and-play image inpainting model with decomposed dual-branch diffusion. In *European Conference on Computer Vision*, 2024. 1, 2, 3, 5, 9, 10
- [24] Sora Kim, Sungho Suh, and Minsik Lee. Rad: Region-aware diffusion models for image inpainting. In *IEEE/CVF Conference on Computer Vision and Pattern Recognition*, 2025. 3
- [25] Yuval Kirstain, Adam Polyak, Uriel Singer, Shahbuland Matiana, Joe Penna, and Omer Levy. Pick-a-pic: An open dataset of user preferences for text-to-image generation. *Advances in neural information processing systems*, 2023. 1, 5, 10
- [26] Weijie Kong, Qi Tian, Zijian Zhang, Rox Min, Zuozhuo Dai, Jin Zhou, Jiangfeng Xiong, Xin Li, Bo Wu, Jianwei Zhang, et al. Hunyuanvideo: A systematic framework for large video generative models. *arXiv preprint arXiv:2412.03603*, 2024. 3
- [27] Kyungmin Lee, Xiahong Li, Qifei Wang, Junfeng He, Junjie Ke, Ming-Hsuan Yang, Irfan Essa, Jinwoo Shin, Feng Yang, and Yinxiao Li. Calibrated multi-preference optimization for aligning diffusion models. In *IEEE/CVF Conference on Computer Vision and Pattern Recognition*, 2025. 3, 4, 14
- [28] Junnan Li, Dongxu Li, Caiming Xiong, and Steven Hoi. Blip: Bootstrapping language-image pre-training for unified vision-language understanding and generation. In *International conference on machine learning*, 2022. 5
- [29] Ruibin Li, Tao Yang, Song Guo, and Lei Zhang. Rorem: Training a robust object remover with human-in-the-loop. In *IEEE/CVF Conference on Computer Vision and Pattern Recognition*, 2025. 3, 15
- [30] Jingyun Liang, Jiezhong Cao, Guolei Sun, Kai Zhang, Luc Van Gool, and Radu Timofte. Swinir: Image restoration using swin transformer. In *IEEE/CVF Conference on Computer Vision and Pattern Recognition*, 2021. 1
- [31] Zhiqiu Lin, Deepak Pathak, Baiqi Li, Jiayao Li, Xide Xia, Graham Neubig, Pengchuan Zhang, and Deva Ramanan. Evaluating text-to-visual generation with image-to-text generation. In *European Conference on Computer Vision*, 2024. 5
- [32] Yaron Lipman, Ricky TQ Chen, Heli Ben-Hamu, Maximilian Nickel, and Matt Le. Flow matching for generative modeling. *arXiv preprint arXiv:2210.02747*, 2022. 1, 2, 3
- [33] Haipeng Liu, Yang Wang, Biao Qian, Meng Wang, and Yong Rui. Structure matters: Tackling the semantic discrepancy in diffusion models for image inpainting. In *IEEE/CVF Conference on Computer Vision and Pattern Recognition*, 2024. 10
- [34] Jie Liu, Gongye Liu, Jiajun Liang, Ziyang Yuan, Xiaokun Liu, Mingwu Zheng, Xiele Wu, Qiulin Wang, Wenyu Qin, Menghan Xia, et al. Improving video generation with human feedback. *arXiv preprint arXiv:2501.13918*, 2025. 1, 3
- [35] Kendong Liu, Zhiyu Zhu, Chuanhao Li, Hui Liu, Huanqiang Zeng, and Junhui Hou. Prefpaint: Aligning image inpainting diffusion model with human preference. *Advances in Neural Information Processing Systems*, 2024. 3, 10

- [36] Andreas Lugmayr, Martin Danelljan, Andres Romero, Fisher Yu, Radu Timofte, and Luc Van Gool. Repaint: Inpainting using denoising diffusion probabilistic models. In *IEEE/CVF Conference on Computer Vision and Pattern Recognition*, 2022. 3
- [37] Nanye Ma, Mark Goldstein, Michael S Albergo, Nicholas M Boffi, Eric Vanden-Eijnden, and Saining Xie. Sit: Exploring flow and diffusion-based generative models with scalable interpolant transformers. In *European Conference on Computer Vision*, 2024. 3
- [38] Nanye Ma, Shangyuan Tong, Haolin Jia, Hexiang Hu, Yu-Chuan Su, Mingda Zhang, Xuan Yang, Yandong Li, Tommi Jaakkola, Xuhui Jia, et al. Scaling inference time compute for diffusion models. In *IEEE/CVF Conference on Computer Vision and Pattern Recognition*, 2025. 5
- [39] Yue Ma, Yingqing He, Xiaodong Cun, Xintao Wang, Siran Chen, Xiu Li, and Qifeng Chen. Follow your pose: Pose-guided text-to-video generation using pose-free videos. In *Proceedings of the AAAI Conference on Artificial Intelligence*, pages 4117–4125, 2024. 2
- [40] Yue Ma, Hongyu Liu, Hongfa Wang, Heng Pan, Yingqing He, Junkun Yuan, Ailing Zeng, Chengfei Cai, Heung-Yeung Shum, Wei Liu, et al. Follow-your-emoji: Fine-controllable and expressive freestyle portrait animation. In *SIGGRAPH Asia 2024 Conference Papers*, 2024.
- [41] Yue Ma, Kunyu Feng, Zhongyuan Hu, Xinyu Wang, Yucheng Wang, Mingzhe Zheng, Xuanhua He, Chenyang Zhu, Hongyu Liu, Yingqing He, et al. Controllable video generation: A survey. *arXiv preprint arXiv:2507.16869*, 2025.
- [42] Yue Ma, Kunyu Feng, Xinhua Zhang, Hongyu Liu, David Junhao Zhang, Jinbo Xing, Yinhan Zhang, Ayden Yang, Zeyu Wang, and Qifeng Chen. Follow-your-creation: Empowering 4d creation through video inpainting. *arXiv preprint arXiv:2506.04590*, 2025.
- [43] Yue Ma, Yulong Liu, Qiyuan Zhu, Ayden Yang, Kunyu Feng, Xinhua Zhang, Zhifeng Li, Sirui Han, Chenyang Qi, and Qifeng Chen. Follow-your-motion: Video motion transfer via efficient spatial-temporal decoupled finetuning. *arXiv preprint arXiv:2506.05207*, 2025. 2
- [44] Yuhang Ma, Xiaoshi Wu, Keqiang Sun, and Hongsheng Li. Hpsv3: Towards wide-spectrum human preference score. *arXiv preprint arXiv:2508.03789*, 2025. 5
- [45] Yue Ma, Xinyu Wang, Qianli Ma, Qinghe Wang, Mingzhe Zheng, Xiangpeng Yang, Hao Li, Chongbo Zhao, Jixuan Ying, Harry Yang, et al. Group editing: Edit multiple images in one go. *arXiv preprint arXiv:2603.22883*, 2026. 2
- [46] Yue Ma, Zhikai Wang, Tianhao Ren, Mingzhe Zheng, Hongyu Liu, Jiayi Guo, Mark Fong, Yuxuan Xue, Zixiang Zhao, Konrad Schindler, et al. Fastvmt: Eliminating redundancy in video motion transfer. *arXiv preprint arXiv:2602.05551*, 2026. 2
- [47] Hayk Manukyan, Andranik Sargsyan, Barsegh Atanyan, Zhangyang Wang, Shant Navasardyan, and Humphrey Shi. Hd-painter: high-resolution and prompt-faithful text-guided image inpainting with diffusion models. In *International Conference on Learning Representations*, 2023. 1, 2, 10
- [48] Alexander Pan, Kush Bhatia, and Jacob Steinhardt. The effects of reward misspecification: Mapping and mitigating misaligned models. *arXiv preprint arXiv:2201.03544*, 2022. 1, 7
- [49] QwenTeam. Qwen3-vl. <https://qwen.ai/blog?id=qwen3-vl>, 2025. Accessed: 2025-11-20. 11
- [50] Alec Radford, Jong Wook Kim, Chris Hallacy, Aditya Ramesh, Gabriel Goh, Sandhini Agarwal, Girish Sastry, Amanda Askell, Pamela Mishkin, Jack Clark, et al. Learning transferable visual models from natural language supervision. In *International conference on machine learning*, 2021. 5
- [51] Rafael Rafailov, Archit Sharma, Eric Mitchell, Christopher D Manning, Stefano Ermon, and Chelsea Finn. Direct preference optimization: Your language model is secretly a reward model. *Advances in neural information processing systems*, 2023. 1, 3
- [52] Robin Rombach, Andreas Blattmann, Dominik Lorenz, Patrick Esser, and Björn Ommer. High-resolution image synthesis with latent diffusion models. In *IEEE/CVF Conference on Computer Vision and Pattern Recognition*, 2022. 2, 10
- [53] Olaf Ronneberger, Philipp Fischer, and Thomas Brox. U-net: Convolutional networks for biomedical image segmentation. In *International Conference on Medical image computing and computer-assisted intervention*, 2015. 1, 3
- [54] Christoph Schuhmann, Romain Beaumont, Richard Vencu, Cade Gordon, Ross Wightman, Mehdi Cherti, Theo Coombes, Aarush Katta, Clayton Mullis, Mitchell Wortsman, et al. Laion-5b: An open large-scale dataset for training next generation image-text models. *Advances in neural information processing systems*, 2022. 5
- [55] John Schulman, Filip Wolski, Prafulla Dhariwal, Alec Radford, and Oleg Klimov. Proximal policy optimization algorithms. *arXiv preprint arXiv:1707.06347*, 2017. 3, 4
- [56] Yutao Shen, Junkun Yuan, Toru Aonishi, Hideki Nakayama, and Yue Ma. Follow-your-preference: Towards preference-aligned image inpainting. *arXiv preprint arXiv:2509.23082*, 2025. 2
- [57] Jascha Sohl-Dickstein, Eric Weiss, Niru Maheswaranathan, and Surya Ganguli. Deep unsupervised learning using nonequilibrium thermodynamics. In *International conference on machine learning*, 2015. 3
- [58] Jiaming Song, Chenlin Meng, and Stefano Ermon. Denoising diffusion implicit models. *arXiv preprint arXiv:2010.02502*, 2020. 3
- [59] Richard S Sutton, Andrew G Barto, et al. *Reinforcement learning: An introduction*. MIT press Cambridge, 1998. 3
- [60] Ashish Vaswani, Noam Shazeer, Niki Parmar, Jakob Uszkoreit, Llion Jones, Aidan N Gomez, Łukasz Kaiser, and Illia Polosukhin. Attention is all you need. *Advances in neural information processing systems*, 2017. 1, 3
- [61] Bram Wallace, Meihua Dang, Rafael Rafailov, Linqi Zhou, Aaron Lou, Senthil Purushwalkam, Stefano Ermon, Caiming Xiong, Shafiq Joty, and Nikhil Naik. Diffusion model alignment using direct preference optimization. In *IEEE/CVF Conference on Computer Vision and Pattern Recognition*, pages 8228–8238, 2024. 1, 3, 12
- [62] Team Wan, Ang Wang, Baole Ai, Bin Wen, Chaojie Mao, Chen-Wei Xie, Di Chen, Feiwu Yu, Haiming Zhao, Jianxiao Yang, et al. Wan: Open and advanced large-scale video generative models. *arXiv preprint arXiv:2503.20314*, 2025. 3

- [63] Jiangshan Wang, Junfu Pu, Zhongang Qi, Jiayi Guo, Yue Ma, Nisha Huang, Yuxin Chen, Xiu Li, and Ying Shan. Taming rectified flow for inversion and editing. *arXiv preprint arXiv:2411.04746*, 2024. 2
- [64] Junke Wang, Zhi Tian, Xun Wang, Xinyu Zhang, Weilin Huang, Zuxuan Wu, and Yu-Gang Jiang. Simplear: Pushing the frontier of autoregressive visual generation through pre-training, sft, and rl. *arXiv preprint arXiv:2504.11455*, 2025. 4
- [65] Peng Wang, Shuai Bai, Sinan Tan, Shijie Wang, Zhihao Fan, Jinze Bai, Keqin Chen, Xuejing Liu, Jialin Wang, Wenbin Ge, et al. Qwen2-vl: Enhancing vision-language model’s perception of the world at any resolution. *arXiv preprint arXiv:2409.12191*, 2024. 5
- [66] Su Wang, Chitwan Saharia, Ceslee Montgomery, Jordi Pont-Tuset, Shai Noy, Stefano Pellegrini, Yasumasa Onoe, Sarah Laszlo, David J Fleet, Radu Soricut, et al. Imagen editor and editbench: Advancing and evaluating text-guided image inpainting. In *IEEE/CVF Conference on Computer Vision and Pattern Recognition*, 2023. 1, 5
- [67] Yikai Wang, Chenjie Cao, Junqiu Yu, Ke Fan, Xiangyang Xue, and Yanwei Fu. Towards enhanced image inpainting: Mitigating unwanted object insertion and preserving color consistency. In *IEEE/CVF Conference on Computer Vision and Pattern Recognition*, 2025. 2, 10
- [68] Yibin Wang, Yuhang Zang, Hao Li, Cheng Jin, and Jiaqi Wang. Unified reward model for multimodal understanding and generation. *arXiv preprint arXiv:2503.05236*, 2025. 4, 5
- [69] Sihao Wu, Xiaonan Si, Chi Xing, Jianhong Wang, Gaojie Jin, Guangliang Cheng, Lijun Zhang, and Xiaowei Huang. Preference alignment on diffusion model: A comprehensive survey for image generation and editing. *arXiv preprint arXiv:2502.07829*, 2025. 1
- [70] Xiaoshi Wu, Yiming Hao, Keqiang Sun, Yixiong Chen, Feng Zhu, Rui Zhao, and Hongsheng Li. Human preference score v2: A solid benchmark for evaluating human preferences of text-to-image synthesis. *arXiv preprint arXiv:2306.09341*, 2023. 1, 5, 10
- [71] Jiazheng Xu, Xiao Liu, Yuchen Wu, Yuxuan Tong, Qinkai Li, Ming Ding, Jie Tang, and Yuxiao Dong. Imagereward: Learning and evaluating human preferences for text-to-image generation. *Advances in Neural Information Processing Systems*, 2023. 5
- [72] Zeyue Xue, Jie Wu, Yu Gao, Fangyuan Kong, Lingting Zhu, Mengzhao Chen, Zhiheng Liu, Wei Liu, Qiushan Guo, Weilin Huang, et al. Dancegrpo: Unleashing grpo on visual generation. *arXiv preprint arXiv:2505.07818*, 2025. 1, 4
- [73] Junkun Yuan, Xu Ma, Defang Chen, Kun Kuang, Fei Wu, and Lanfen Lin. Label-efficient domain generalization via collaborative exploration and generalization. In *Proceedings of the 30th ACM international conference on multimedia*, pages 2361–2370, 2022. 3
- [74] Junkun Yuan, Xu Ma, Defang Chen, Kun Kuang, Fei Wu, and Lanfen Lin. Domain-specific bias filtering for single labeled domain generalization. *International Journal of Computer Vision*, 131(2):552–571, 2023. 2
- [75] Junkun Yuan, Xu Ma, Defang Chen, Fei Wu, Lanfen Lin, and Kun Kuang. Collaborative semantic aggregation and calibration for federated domain generalization. *IEEE Transactions on Knowledge and Data Engineering*, 35(12):12528–12541, 2023. 2
- [76] Junkun Yuan, Xinyu Zhang, Hao Zhou, Jian Wang, Zhongwei Qiu, Zhiyin Shao, Shaofeng Zhang, Sifan Long, Kun Kuang, Kun Yao, et al. Hap: Structure-aware masked image modeling for human-centric perception. *Advances in Neural Information Processing Systems*, 2023. 2
- [77] Kai Zhang, Lingbo Mo, Wenhui Chen, Huan Sun, and Yu Su. Magicbrush: A manually annotated dataset for instruction-guided image editing. *Advances in Neural Information Processing Systems*, 2023. 1
- [78] Lvmin Zhang, Anyi Rao, and Maneesh Agrawala. Adding conditional control to text-to-image diffusion models. In *IEEE/CVF Conference on Computer Vision and Pattern Recognition*, 2023. 2, 10
- [79] Richard Zhang, Phillip Isola, Alexei A Efros, Eli Shechtman, and Oliver Wang. The unreasonable effectiveness of deep features as a perceptual metric. In *IEEE/CVF Conference on Computer Vision and Pattern Recognition*, 2018. 15
- [80] Junhao Zhuang, Yanhong Zeng, Wenran Liu, Chun Yuan, and Kai Chen. A task is worth one word: Learning with task prompts for high-quality versatile image inpainting. In *European Conference on Computer Vision*, 2024. 1, 2, 10

Appendix

A. More Results on Reward Model Bias Studies



(a) A cartoon drawing of a kitchen.



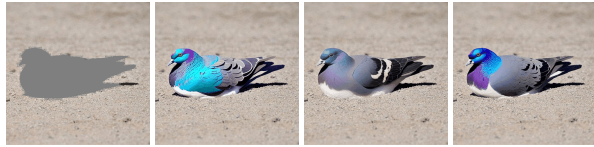
(c) A couch with pillows and a wall behind it.



(e) A house floating in the air over a lake.



(g) A vase filled with colorful flowers on a table.



(i) A pigeon is sitting on the ground.



(k) A sheep with pink fur is standing.



(m) A lamb standing in a field of green grass.



(o) A vase with some flowers in it.



(b) A pink lotus flower blooming with green leaves.



(d) A dog sitting on the beach.



(f) Sunflowers in a vase with pears on a table.



(h) A notebook, glasses and a camera on a map.



(j) A purple chair with a black seat and back.



(l) A teacup and saucer with spoons.



(n) A vase with blue flowers sitting on a table.



(p) A kitten is playing with a flower.

Figure 11. **More results on reward model bias studies using BrushNet.** In each sub-figure, the four images (from left to right) display: the *masked image*, followed by inpainting results from models trained using *HPsV2*, *PickScore*, and *Ensemble*. For optimal detail, view figures zoomed in.



(a) A woman in white holding a bouquet of flowers.



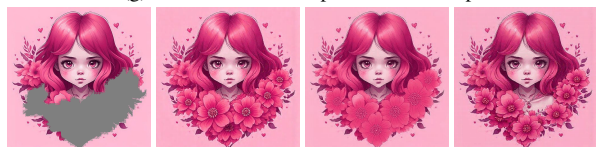
(c) Wolf howling at the moon.



(e) A couch with a winged chair at a window.



(g) A fruit bowl with a pink flower on top.



(i) A girl with pink hair and flowers on her face.



(k) A lamp and a cup of tea on a table.



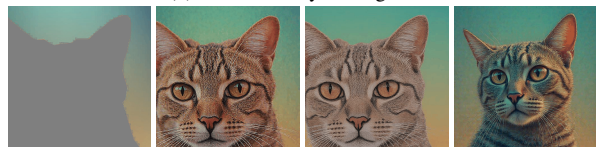
(m) A rabbit sitting on a hill with trees.



(o) A teacup and saucer with spoons.



(b) A cartoon boy driving a car.



(d) A cat is shown in low polygonal style.



(f) A bright moon on the sea.



(h) A small cabin in the snow near a lake.



(j) Cartoon fox driving a car with a cute face.



(l) A person standing on a tile floor with a rug.



(n) A red cabin sits on the shore of a lake.



(p) A vase with flowers in it on a dark background.

Figure 12. **More results on reward model bias studies using FLUX.1 Fill.** In each sub-figure, the four images (from left to right) display: the *masked image*, followed by inpainting results from models trained using *HPSv2*, *PickScore*, and *Ensemble*. For optimal detail, view figures zoomed in.



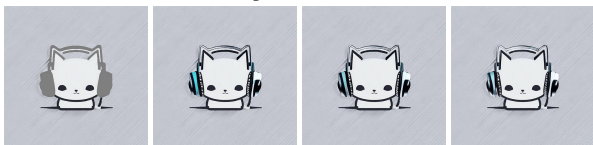
(a) a cartoon giraffe sitting down and looking at the camera



(c) a cup of tea sits on top of a wooden table



(e) a couch with pillows and a wall behind it



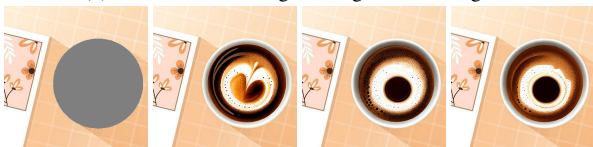
(g) a cat with headphones on its head



(i) a chair in front of a wall with a floral pattern



(k) a white rabbit sitting on the ground in the grass



(m) a cup of coffee and a notebook on a table



(o) a cup of coffee on a table next to a window with the moon and stars in the sky



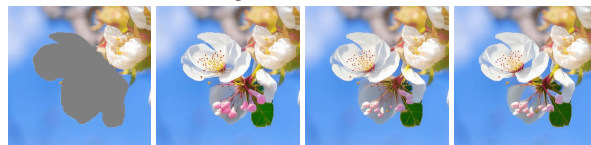
(b) a house in the middle of a foggy night



(d) a fairy with a lantern in her hand



(f) a cartoon drawing of a kitchen with a stove and oven



(h) a close up of a cherry blossom with white flowers



(j) wind turbines are seen in the ocean near a pier



(l) a lighthouse in the middle of a stormy sea



(n) a cartoon rabbit wearing a blue coat and hat

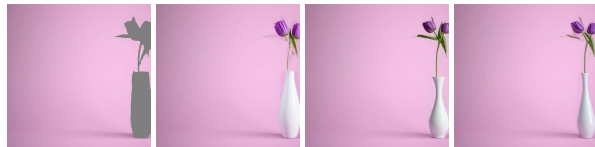


(p) a woman standing in front of a large spaceship

Figure 13. **More results on Ensemble bias studies using BrushNet.** In each sub-figure, the four images (from left to right) display: the *masked image*, followed by inpainting results from models trained using *Ensemble*, *CaPO*, and *CaEN*. For optimal detail, view figures zoomed in.



(a) cartoon fox driving a car with a cute face



(c) a white vase with purple tulips in it



(e) a blue butterfly with stars on it



(g) a house floating in the air over a lake



(i) a blue bird sitting on a branch with yellow flowers



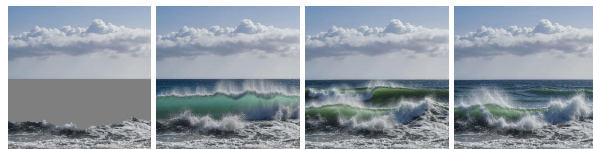
(k) a green velvet chaise with studded backrest on a dark background



(m) a cute little rabbit with a bow on its back



(o) a painting of a house with a full moon in the sky



(b) a large wave crashing into the ocean with white clouds in the sky



(d) a person holding a stopwatch with the words 2020 and 2021



(f) a man and woman standing on rocks with a fish in the water



(h) a couch with a winged chair in front of a window



(j) the cover of the book, the girl and the dog



(l) a woman in a red hat and red dress



(n) a white shelf with books and other items on it



(p) anime girl

Figure 14. **More results on Ensemble bias studies using FLUX.1 Fill.** In each sub-figure, the four images (from left to right) display: the *masked image*, followed by inpainting results from models trained using *Ensemble*, *CaPO*, and *CaEN*. For optimal detail, view figures zoomed in.